Norwegian University
of Life Sciences

Master's Thesis 2020 30 ECTS
Faculty of Science and Technology

Analysing the effect of neural morphology on extracellular spikes

Jørgen Hoel
MSc. Environmental Physics and Renewable Energy

This page is intentionally left blank.

Acknowledgements

This piece of paper marks the completion of my Master's degree at the Norwegian University of Life Sciences, and the end of my studies in Ås. The journey has been both fun and challenging, and I would like to express my appreciation to all the people who have supported me along the way.

Thanks to my supervisors, Torbjørn V. Ness and Gaute T. Einevoll, for all the help and encouragement you have given me. Special thanks to Torbjørn for giving many ideas and advice on the manuscript and always keeping his door open.

Thanks also to all my family and friends for sharing all the good conversations and good laughs throughout my time here. The hurdles would have been many times taller without you.

Ås, June 2nd, 2020

Jørgen Hoel

Abstract

A common method of measuring neural activity is to insert recording electrodes into brain tissue, as active neurons cause changes in the extracellular potential. Such experiments have been instrumental to neuroscience, having furthered our understanding of the underlying mechanisms of the brain. In some studies, far fewer neurons have been detected to fire in electrode recordings than expected, leading to a "dark matter problem" in the brain being proposed.

Computer simulations can be used to get insight into the connection between firing neurons and extracellular signals. Theory developed in Pettersen and Einevoll (2008) [1] for idealised neuron models suggests a connection between the maximum extracellular spike amplitude from a firing neuron and its basic structure. We apply the theory to a large database of more complicated models to investigate whether it can be further generalised, and explore a possible explanation of the dark matter problem; that a relevant number of neurons are undetectable with extracellular recording electrodes.

Using the neuroinformatics tool LFPy, we simulate extracellular action potentials (EAP) from individual cell models. Previously developed digitally reconstructed neuron models from rat neocortex were used. We find that the theory generalises well to more complicated neuron models. We encountered and investigated systematic differences in EAP amplitude between excitatory and inhibitory neurons with similar structural properties. The investigation was done using simpler idealised models, and we found the EAP amplitude to be dependent on the number of dendrites connected to the soma. As nearly all reconstructed models were found to be detectable, we conclude that the dark matter problem is unlikely to be caused by large numbers of cells being unmeasurable with extracellular electrodes.

Sammendrag

En ofte brukt metode for å måle nevral aktivitet er ved måleelektroder plassert i hjernevev, ettersom aktive nevroner påvirker det ektracellulære potensialet. Slike eksperimenter har vært instrumentale i nevrovitenskapen, og har utviklet vår forståelse av de underligende mekanismene i hjernen. I noen studier er langt færre nevroner blitt målt enn forventet, noe som har ført til at et mulig "mørk materie"-problem i hjernen er blitt foreslått.

Datasimuleringer kan brukes til å få innsikt i sammenhengen mellom aktive nevroner og ekstracellulære signaler. Teori utviklet i Pettersen og Einevoll (2008) [1] for idealiserte nevronmodeller antyder en sammenheng mellom ekstracellulær maksimalamplitude fra et fyrende nevron og dens grunnleggende struktur. Vi anvender teorien på en stor database med mer komplekse modeller for å undersøke om den kan generaliseres videre, og utforsker en mulig forklaring på "mørk materie"-problemet; at en relevant mengde nevroner er udetekterbare med ekstrecellulære målelektroder.

Vi simulerer ekstracellulære aksjonspotensialer (EAP) ved hjelp av nevroinformatikkverktøyet LFPy. Tidligere utviklede digitalt rekonstruerte nevronmodeller fra rotters neocortex ble brukt. Vi erfarer at teorien generaliserer bra til de mer kompliserte modellene. Vi støtte på, og utforsket systematiske forskjeller i EAP amplitude mellom eksitatoriske og inhibitoriske nevroner med like strukturelle egenskaper. Utforskningen ble gjort ved bruk av enklere idealiserte modeller, og vi fant at EAP-amplituden avhenger av antallet dendritter tilkoblet soma. Ettersom vi fant at nesten alle de rekonstruerte modellene er detekterbare, konkluderer vi med at det er usannsynlig at "mørk materie"-problemet skyldes at et stort antall nevroner ikke kan måles av ekstracellulære måleelektroder.

Contents

List of Figures

List of Tables

Chapter 1

Introduction

We have understood for a long time that the brain serves an essential function to our experience. Archaeological findings suggest that even prehistoric humans had notions that the brain is central to our beings, as 7000 year old skulls carried marks of attempted surgeries [2]. Today we know that the brain is where thoughts arise, that it is where memories are stored, and that it functions as the control center of the body. It sends and receives signals, and in short makes our bodies do what they do [3]. Understanding how consciousness and complex thoughts are formed on a fundamental level however, is a milestone that neuroscience has not yet reached [4].

The cerebral cortex is the outermost part of the mammalian brain, and is the largest part of the human brain. Quantitatively speaking, most of our knowledge of the brain stems from studies in cortex [5]. The neocortex is the largest portion of the cortex, and is involved in many higher-order functions such as sensory perception, cognition, and sophisticated motor control [3]. It is divided into six layers that are distinguished by neuron types and neuronal connections, labeled I-VI, from outermost to innermost. Connections go between neurons in the same layer, between neurons in different layers, and to entirely different regions of the brain. The neocortex is believed to be divided into minicolumnns, vertical chains of neurons that serve as functional units [6].

Recording electrodes allow neurophysiologists to measure activity in the brain, as neurons communicate by sending electrical pulses [2]. Methods come with a varying degree of invasiveness, from electrodes being placed on top of the scalp or electroencephalography (EEG), on top of cortex or electrocorticography (ECoG), or inside the neuronal tissue [5]. While EEG naturally records from a very large

number of neurons, inserted electrodes can pick up signals from only a handful of neurons at a time. The recordings from tissue can be split into two parts; the low frequency ($< 500\,Hz$) part is generated by many neurons in the neighbourhood of the electrode and is called local field potential (LFP), while the high-frequency ($> 750\,Hz$) part is referred to as multi-unit activity (MUA) and picks up activity from a few closer neurons [7].

Extracellular electrode recordings of neuronal signals have played crucial parts to the development of neuroscience and our understanding of the fundamental mechanisms of the brain. Experiments with electrodes in cat striat cortex by Wiesel and Hubel (1959) revealed information about how visual stimuli are processed [8]. In a more recent example, electrode recording in rat cortex shed light on spatial representation in the brain [9]. As the firing of electrical pulses is key to neuronal communication, it is natural to presume that nearly every living neuron will be observed to fire given a long time of observation. However, reports from several experiments with electrode recordings show a low rate of neurons being active, leading to a proposed "dark matter problem" in the brain [10]. That is, why are so many neurons seemingly silent? In one instance, in experiments from rat hippocampus 10-100-fold fewer neurons were recorded from than expected from the neuronal density [10]. One potential explanation could be that some neurons do not produce measurable extracellular potentials.

Here we use computer simulations of individual neuron models to determine their detectability, and analyse effects of neuron structure on the amplitude of extracellular signals. In particular, the dependence on a morphology factor, suggested in Pettersen and Einevoll (2008) was analysed [1]. Digitally reconstructed neuron models from the EPFL Blue Brain Project [11, 12], and simplified, idealised models were used. By determining a spatial range of detectability for each cell model, estimates of how many neurons one can expect to find with electrodes inside neocortex were produced. The results suggest a strong relationship between the maximum signal amplitude and the morphology factor, but also displayed an unexpected difference between excitatory and inhibitory neurons. Simulations done on idealised models suggest that the number of dendrites attached to the soma could be an explanatory factor, as the excitatory neurons on average had more dendrites connected to the soma. As nearly every cell model in the Blue Brain set produced significant extracellular spike amplitudes, we find it unlikely that the dark matter problem in the brain is caused by a large number of cells being undetectable.

Chapter 2

Theory

2.1 The neuron

Neurons, often referred to as brain cells, transmit signals in the brain and around the body. These signals are caused by ions, electrically charged particles, that flow in and out of neurons. Glial cells are the other main type of cells in the brain, and their functions include providing nutrients and protection for the neurons [2, 3]. The human brain contains about 86 billion neurons, about 16 billion of them located in the cerebral cortex [13].

A neuron consists of a main body, the soma, and several elongated bodies, axons and dendrites, as illustrated in Figure 2.1. The cell is confined by a lipid bilayer that keeps ions from travelling freely across the cell membrane. The layer thus acts much like an electrical capacitor [2]. Ion pumps and ion channels on the cell surface make it so that the inside of the cell rests at about $-65\,\mu V$ [14]. Axons and dendrites connect neurons together by allowing electrical signals to be carried from one neuron to another. Connections typically go from axon to dendrite, so that the axons transmit signals and the dendrites receive them [3].

The transmission of signals between neurons happens through channels known as synapses. They are located on both the sending and receiving cell, referred to as the presynaptic and postsynaptic cell respectively. There are two types of synapses, distinguished by whether they transfer the signal electrically or chemically. When chemical synapses are activated, they release neurotransmitters, signalling chemicals, that diffuse across the gap between cells, causing ion channels to open

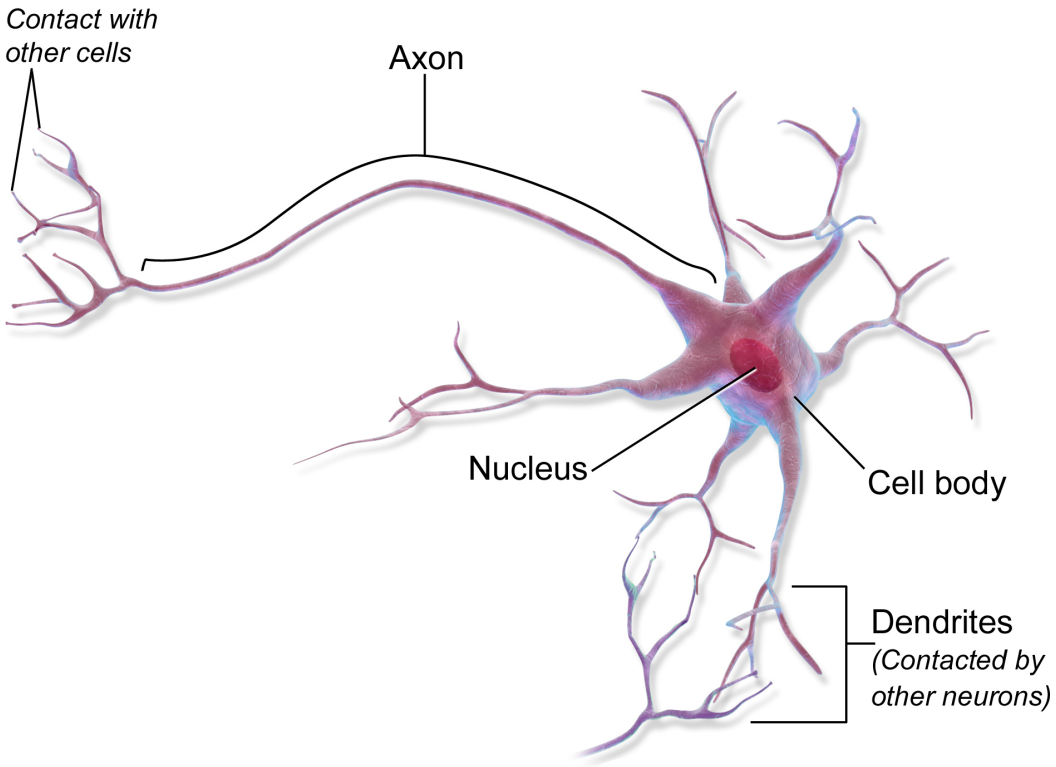

Figure 2.1: Illustration of a neuron, with the soma (Cell body), dendrites and axons specified. The soma contains the nucleus and other organelles. The synapses are located at the contact points, from which the cell sends and receives signals to and from other cells. Adapted from Blausen.com staff (2014). "Medical gallery of Blausen Medical 2014". WikiJournal of Medicine 1 (2). DOI:10.15347/wjm/2014.010. ISSN 2002-4436

on the postsynaptic cell. The electrical synapse connects the neurons physically by gap junctions that allow ions to flow directly from the presynaptic to the post-synaptic side [2].

If the potential across the cell membrane reaches a certain threshold, the neuron will fire an action potential. The action potential is a quick depolarisation and repolarisation of the membrane potential, that moves down the axon, activating synapses as it travels. This is commonly referred to as a spike, and a neuron firing an action potential is said to be spiking [2]. It is caused by ion channels that are voltage-gated, meaning they are activated as the membrane potential reaches a threshold [15].

Neurons are labeled as either excitatory or inhibitory based on the change in membrane potential they cause on postsynaptic cells. Excitatory neurons cause an increase of potential on the postsynaptic side and inhibitory neurons decrease it [16]. While it is possible for a neuron to act both excitatory and inhibitory, it is rare, as in general all axonal branches release the same neurotransmitters [17]. Although the ratio varies between regions of the brain, excitatory neurons are usually more abundant than inhibitory ones, the brain average being about 80 % excitatory cells [3].

2.2 Modelling extracellular potentials

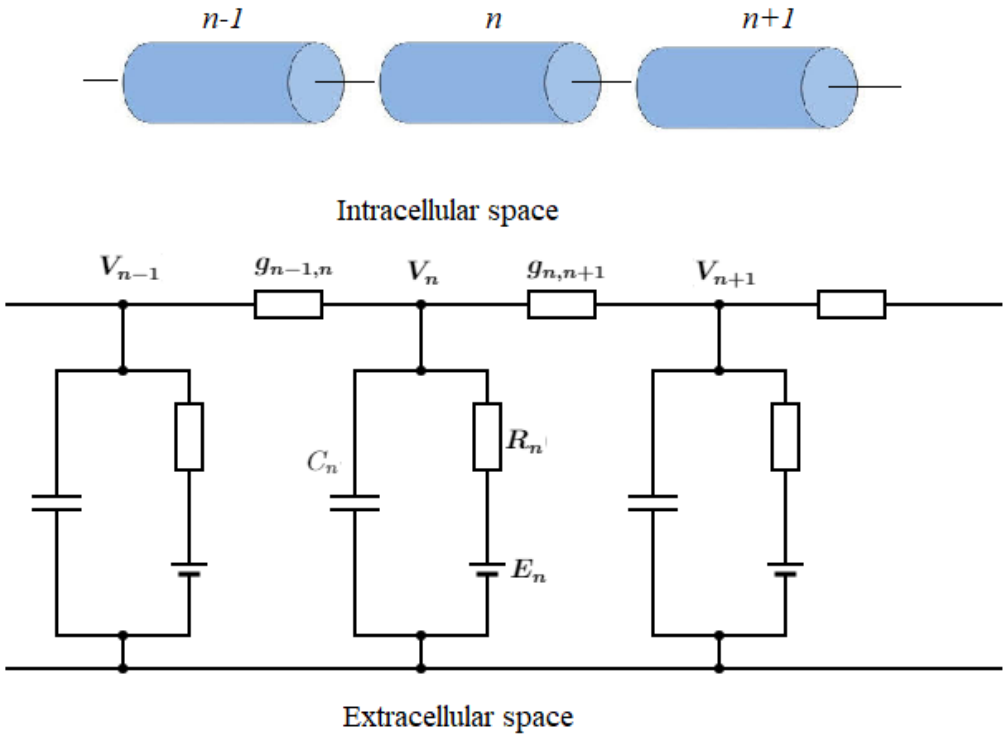

Figure 2.2: A section of a neuron modelled as connected cylindrical compartments (top) and electrical RC-circuits (bottom). Compartment n has membrane potential V_n, capacitance C_n, resting potential E_n, and membrane resistance R_n. $g_{n,n+1}$ and $g_{n-1,n}$ represents the axial conductance between compartment n and compartments $n+1$ and $n-1$ respectively.

When a neuron fires an action potential, the spike can generally be detected by

recording electrodes outside of the cell. The signals are referred to as extracellular action potentials (EAP). The change in potential in the extracellular region is caused by charges flowing across the neuronal membrane. Simulating the change in extracellular potential caused by a neuron is therefore doable by first computing its transmembrane currents, which can be done by multicompartmental modelling [14]. The neuron is modelled as many sub-units (compartments) that are sufficiently small so that the membrane potential of any one compartment is approximately uniform. The soma is taken as a spherical compartment, and axons and dendrites are represented by strings of cylinders. Every compartment is modelled as a resistor–capacitor circuit as illustrated in Figure 2.2. For compartment n with membrane potential V_n, capacitance C_n, resting potential E_n and membrane resistance R_n the equation

$$(V_{n+1} - V_n) - g_{n-1,n}(V_n - V_{n-1}) = C_n \frac{dV_n}{dt} + \sum_j I_n^j, \tag{2.1}$$

can be derived [14]. $g_{n,n+1}$ and $g_{n-1,n}$ represent the axial conductances between compartment n and compartments $n+1$ and $n-1$ respectively. $\sum_j I_n^j$ is the net contribution of the ionic channels on the membrane. Eq. (2.1) follows from Kirchoff's law of currents, stating that the charge leaving a node is equal to the charge entering it. As the left hand side is the difference between the intracellular charge entering and leaving the compartment, the right hand side equals the total transmembrane current I_n [18].

The potential change in a medium caused by charge entering or leaving a point source can be determined by volume conductor theory [19]. Assuming an electrically isotropic uniform medium of infinite size, charge will flow equally in all directions into or from the point source. By further assuming that the medium is ohmic and that quasistatic approximations of Maxwell's equations are valid, the contribution to extracellular potential at position $\boldsymbol{r}$ from a point source of strength $I_n(t)$ at position $\boldsymbol{r_n}$ and time t is

$$\phi(\boldsymbol{r}, t) = \frac{1}{4\pi\sigma} \frac{I_n(t)}{|\boldsymbol{r} - \boldsymbol{r_n}|}\,, \tag{2.2}$$

where σ is the conductance of the tissue [20]. By the assumption of the medium being ohmic, contribution from multiple sources add linearly [19]. Thus, when measuring signals from n point sources, the net contribution to potential becomes

$$\phi(\boldsymbol{r}, t) = \frac{1}{4\pi\sigma} \sum_{n=1}^{N} \frac{I_n(t)}{|\boldsymbol{r} - \boldsymbol{r_n}|}. \tag{2.3}$$

When modelling the extracellular potential, the somatic contribution can be approximated by taking the current to be entering and leaving a single point in space. This is called a *point-source* approximation. For an axonal or dendritic compartment, the contribution can be computed by assuming the transmembrane currents to be equally distributed, and integrating Eq. 2.3 along its length. This method is referred to as *line-source* approximation [21, 22].

2.3 Amplitude of extracellular action potentials

The structure of a neuron will necessarily affect the shape and size of the EAP. For instance, for a neuron consisting only of a point soma, firing will cause no change in extracellular potential. This follows from the linear summation of potentials in Eq. (2.3) and Kirchhoff's current law, as the net current in and out of the membrane would be of the same size and located at the same spot.

In the case of an idealised ball-and-stick neuron, a simplified model consisting of a spherical soma and one cylindrical dendrite, it was shown that the maximum extracellular potential is dependent on the soma radius r_s and the dendrite diameter d [1]. Specifically, for a neuron with dendritic axial resistance R_i, membrane resistance R_m and membrane capacitance C_m in a medium of conductivity σ, it was found that

$$|\boldsymbol{T}_{near}| = \frac{1}{4\sigma r} \frac{d^{3/2}|\boldsymbol{s}|}{2\sqrt{R_i R_m}} \propto \frac{d^{3/2}\sqrt{\omega\tau}}{\sigma r \sqrt{R_i R_m}} \propto \frac{d^{3/2}}{\sigma r} \sqrt{\frac{f C_m}{R_i}}, \tag{2.4}$$

where $\boldsymbol{T}_{near}$ is a complex transfer function of the extracellular potential near the soma, r is the distance from soma center and $\boldsymbol{s} = \sqrt{1 + j\omega\tau}$ is a complex number relating to the phase of the potential. Here, ω is the angular frequency of the signal and $\tau = R_m C_m$ is the membrane time constant. To derive the proportionalities, the facts that $|\boldsymbol{s}| = ((\omega\tau)^2 + 1)^{1/4}$ and $\omega = 2\pi f$, with f being the signal frequency, were used [1]. From this it follows that the largest amplitude will be recorded immediately outside of soma, where $r = r_s$. Assuming small variability in the parameters of the cell materials, C_m and R_i, within a set of cells, it follows that

$$|\boldsymbol{T}_{max}| \quad \lesssim \quad \frac{d^{3/2}}{r_s}, \tag{2.5}$$

within the set. As the arguments leading up to 2.4 do not depend on there being a single dendrite [1], 2.5 can be modified to

$$|\boldsymbol{T}_{max}| \quad \lesssim \quad \frac{\sum_{i=1}^{n} d_i^{3/2}}{r_s}, \tag{2.6}$$

in the case of there being n dendrites connected to the soma.

Chapter 3

Methods

3.1 NEURON and LFPy

NEURON is a software developed for computationally efficient simulations of individual neurons and networks of neurons. It includes tools for constructing compartmental neuron models, done by specifying the locations and connection points of the compartments [18]. LFPy is a python-package reliant on NEURON, and can be used for computation of extracellular potentials by multicompartmental modelling [21, 23], as reviewed in section 2.2. It was used in all simulations of this project.

3.2 Cell models

3.2.1 Reconstructed models

Simulations were carried out on digitally reconstructed neurons from juvenile Wistar (Han) rat somatosensory cortex, developed by the EPFL Blue Brain Project [11, 12]. The models were downloaded from the Neocortical Microcircuit Collaboration Portal [24]. The portal also provides data of neuron densities and numbers of neuronal types in the microcircuit, which were used to make the estimates in sec. 4.1. Every neuron is labelled according to its layer, morphological type, and electrical type by conventions established by the Blue Brain research team. There

are 207 distinct morpho-electrical subtypes in the microcircuit, with 5 example models for each subtype available [24]. An example of model L5_TTPC1_cADpyr is plotted in Fig 3.1A. The process of loading the models was helped by the example script 'example_EPFL_neurons.py' available from LFPy [23].

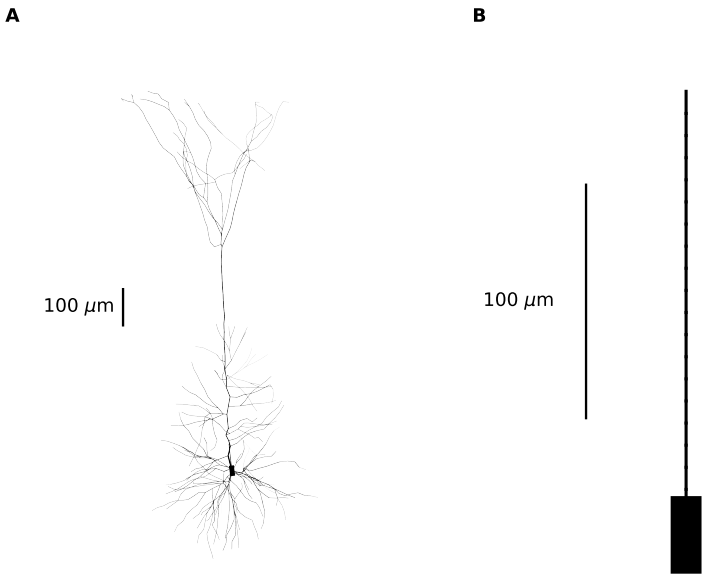

Figure 3.1: **A**: Model L5_TTPC1_cADpyr from the Blue Brain Projects digital reconstruction of a microcircuit from Wistar rat cortex. **B**: Example of an idealised models. This example, consisting only of one dendrite on the soma, is referred to as a ball-and-stick model.

3.2.2 Idealised models

To investigate findings from simulations on the complex reconstructed models, simpler idealised models were used. The idealised models were constrained to only having dendrites connected to the soma. Ten models were created with 1-10 dendrites. Every dendrite was given the same length of 140 μm, and were symmetrically distributed on the soma. The simplest model, with only one dendrite (ball-and-stick model) is illustrated in 3.1B.

3.3 Simulation

After being loaded, the reconstructed models were rotated such that that the apical dendrite of a pyramidal neuron lied along the z-axis, with the soma center at origin. To measure extracellular potentials, virtual recording electrodes were placed at various distances from the soma on the xy-plane. The potential recorded from an electrode is computed as the average potential of several points on a disk facing the soma center. Disks of radius $5\,\mu m$ with 50 points were used. For a given distance from the soma center, the recordings from four electrodes placed along the x- and y-axis were averaged to smoothen the output, reducing the impact of abnormalities such as recording very close to a dendrite. In analysis of results, a detection threshold of $30\,\mu V$ was used, similar to in Buccino et al. (2018) [25]. EAPs lower than this were taken to be undetectable by an electrode recording *in vivo*.

The following two subsections explain the methods used to simulate spikes in neurons. Simulations lasted $15\,ms$ in both cases, with neurons set to fire once during this time. Scripts used for simulation and visualisation of results are available from github at: `github.com/jorgenhoel299`.

3.3.1 Synaptic input

Feeding charge into a cell model is a straightforward way of making it spike, as neurons fire action potentials automatically when the potential across the membrane reaches a certain threshold in the soma region. This was done in LFPy by placing a synapse at the soma and setting the input strength sufficiently high so that the neuron spikes after a short time. We refer to this method as *synaptic input*.

3.3.2 Voltage clamping

Another way of simulating a spiking neuron is to force a predetermined spike in the model, similar to in Pettersen and Einevoll (2008) [1]. This is analogous to the use of a voltage clamp on real neurons, by which the membrane potential of the cell is controlled [15]. For the reconstructed models, this was done by recording the somatic voltage from a spiking layer V pyramidal neuron, L5_TTPC1_cADpyr, activated by synaptic input. The recorded spike was then used on this model

and all other reconstructed models, thus giving each cell approximately the same somatic voltage during the simulations. Voltage dependent ion channels, that would under normal circumstances be instrumental to the generation of an action potential, were turned off so as not to change the spike. For the idealised neurons, somatic voltage from a ball-and-stick model was used. The reconstructed and idealised model used to record and store somatic voltage are plotted in Figure 3.1A and B respectively. Although imposing a membrane potential on the neuron is quite different from the real firing process, it makes comparing the EAP from cells of different types easier, since they have the same intracellular spike [1].

Chapter 4

Results

Extracellular action potentials (EAP) from every neuron model used in the reconstructed microcircuit [11] were recorded by both synaptic input and voltage clamping. The setup is illustrated in Fig 4.1. Results showed only quantitative differences between the two methods, see Figures 4.5 and 4.6 for comparisons. Average EAP amplitudes for excitatory and inhibitory neurons in each layer is plotted against distance from soma in Figure 4.2, showing an exponential decrease in amplitude with distance. Noticeably, excitatory neurons produce consistently higher amplitudes than inhibitory neurons. At 30 μm outside the center of soma, most cells would be invisible assuming a detection threshold of 30 μV. Excitatory neurons in Layer V are the exception, having much larger amplitudes then the other groups at close range.

The maximum recordable EAP of a cell was taken as the potential measured 1 μm outside the soma surface. Results from every cell model using voltage clamping is shown by layer in Figure 4.3. Again the smallest amplitudes belong to inhibitory neurons, and the largest amplitudes to excitatory neurons (with the exception of layer I, as it has only inhibitory cells). Using the detection threshold of 30 μV, only six cell models in the microcircuit would be undetectable, their maximum amplitudes being about 20 μV. These six are all in layer IV of BP morphology. They constitute a microscopic fraction of the total neurons, as there are only 8 L4_BP neurons vs a total of 4,656 neurons in layer IV. Thus, nearly every neuron in the microcircuit would be detectable by inserted electrodes if placed at 1 μm distance. Nevertheless, this suggests that it is possible for some neurons to be undetectable with extracellular electrode recordings.

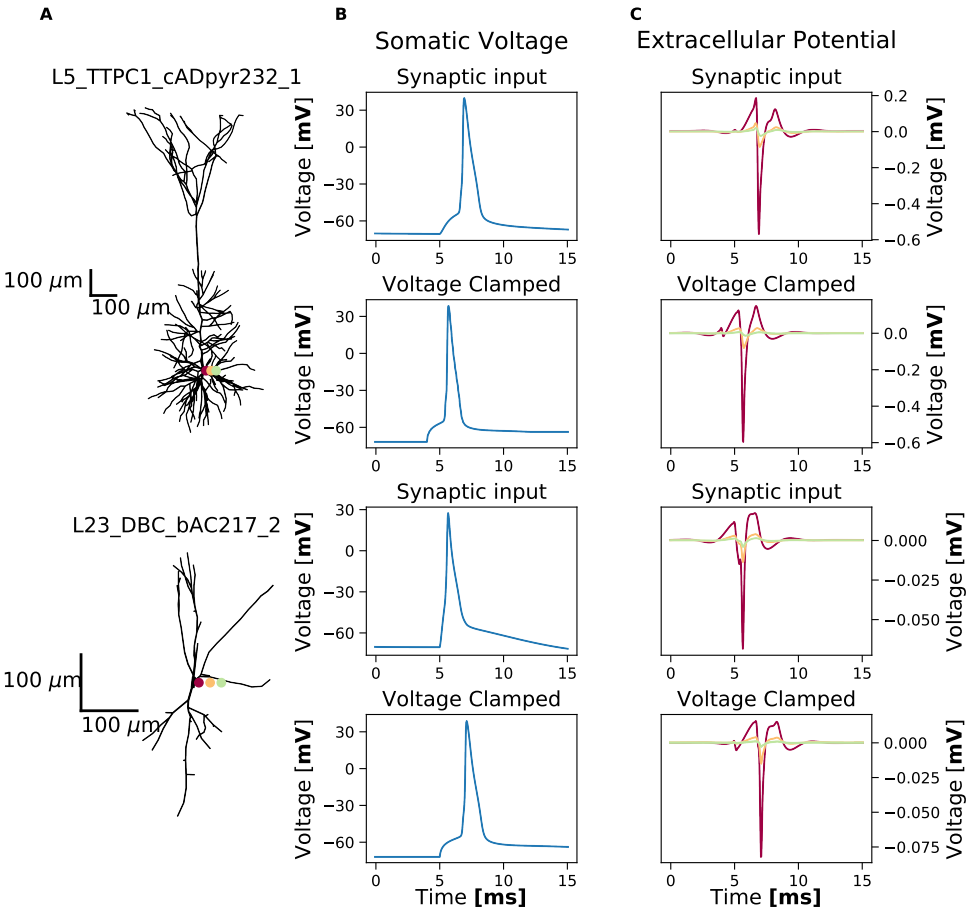

Figure 4.1: **A**: Two reconstructed cell models from the Blue Brain dataset. The colored circles represent locations of recording electrodes. In simulations, outputs from four electrodes placed symmetrically at the same distance from soma center were averaged. **B**: Voltage in soma during simulation. **C**: Extracellular potential during simulation. The colors of the plots correspond to the colored electrodes in **A**. Spike amplitudes are taken as half the difference between the highest and lowest voltage of the recorded signals. The first and third plot in **B** and **C** are from simulations with synaptic input, and the second and fourth plots are from simulations with voltage clamping.

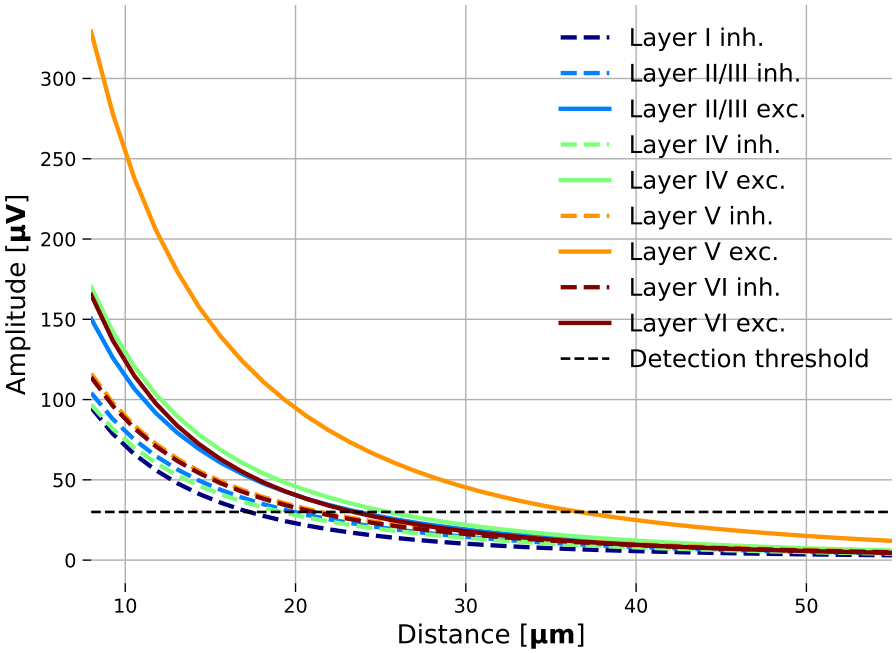

Figure 4.2: Average amplitude of inhibitory and excitatory neurons in every layer by distance from soma center. Results from voltage clamped cells are shown, but the recordings from synaptic input gave similar results. Note that layer I does not have excitatory neurons, and that every line starts at the same distance, 8 μm. This is slightly larger than the largest soma radius of all models in the Blue Brain set.

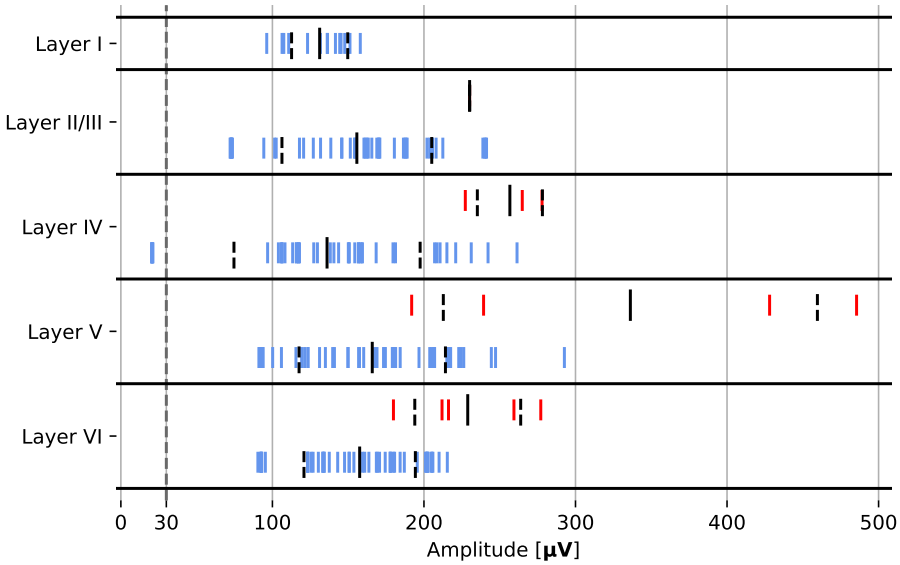

Figure 4.3: Maximum extracellular amplitude for every neuron model in the Blue Brain microcircuit as simulated by voltage clamping. The blue and red bars represent inhibitory and excitatory neurons respectively. The black bars are the means of all neurons of the type in the layer, and the dotted bars represent one standard deviation. The dotted grey line at 30 μV represents a detection threshold. Results from synaptic input were similar and are not included.

4.1 Detectable range of reconstructed models

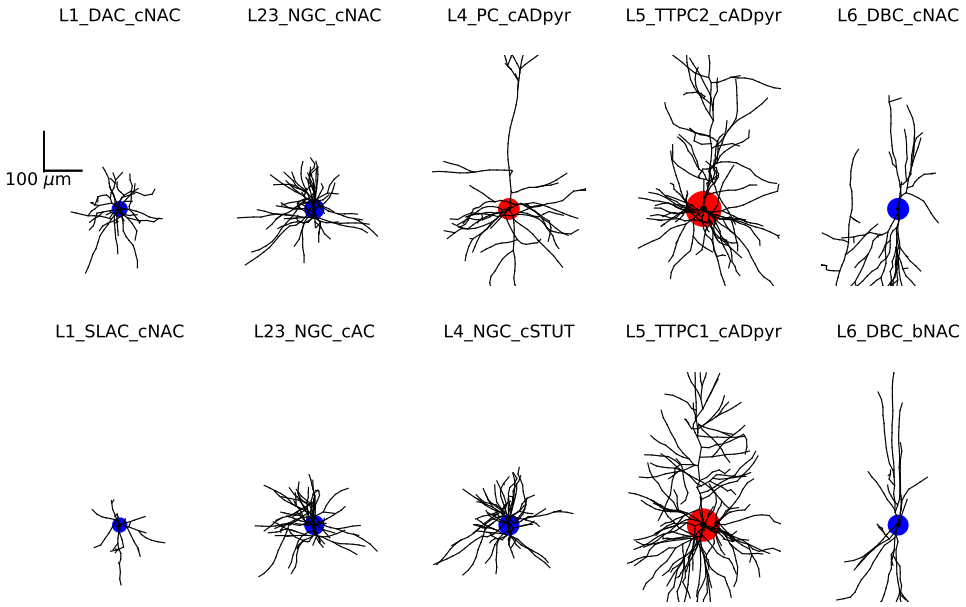

Figure 4.4: Two neurons from every layer in the microcircuit with spatial range of detectability plotted around soma. The two neurons with the largest detectable ranges was chosen from each layer. The range is visualised in red for excitatory neurons and in blue for inhibitory neurons. The ranges were calculated from simulations with voltage clamped cells, taking 30 μV as a threshold of detection.

Estimates of how many neurons one would expect to record from are presented for each layer. To make the estimates, the numbers of instances of each neuron in the microcircuit were scaled with neuron densities in the layers to estimate the density of every neuron. To illustrate with an example: the model L5_TTPC1_cADpyr makes up about 40 % of cells in layer V. Layer V has a neuronal density of $83,900 neurons/mm^3$ [24], meaning that L5_TTPC1_cADpyr has a density of $\approx 33,500 neurons/mm^3$ in layer V. By placing electrodes at increasingly larger distances during simulations, a detectable spatial range for every neuron was determined, equal to the largest distance from the soma center at which the EAP is still larger then the detection threshold of $30 \mu V$. A detectable volume is approximated by a sphere centered in soma center, with radius equal to the detectable range of the cell. Some cells and their detectable volumes are shown in Fig 4.4. Assuming every neuron fires at least once during an *in vivo* recording, the expected

number of neurons to pick up with electrodes in a layer with k neurons is

$$E[N] = \sum_{i=1}^{k} \sigma_i * V_i, \tag{4.1}$$

where σ_i and V_i are the density and detectable volume of neuron i respectively.

The analysis shows that the expected number of neurons to be recorded is heavily dependent on the electrode position in neocortex. In layer V, we expect to detect about 22 and 28 cells with voltage clamping and synaptic input respectively. This is almost equal to all the other layers combined. Excitatory neurons are far more likely to be detected than inhibitory neurons in all layers (except in layer I), the main factor being that they are far more numerous in the microcircuit. A visualisation of electrode depth in neocortex and expected number of recorded neurons is presented in Figure 4.5. The analysis assumes that instances of every neuron is homogeneously distributed in its layer, and an arbitrary placement of recording electrode. Note that a common practice in experiments on live cells is to initially manoeuvre the electrode until a strong signal is detected. The results suggest that the ratio of measured excitatory to inhibitory cells will be higher than their real representation in the circuit for all layers, see Table 4.1.

Table 4.1: Ratio of excitatory to inhibitory cells present in each layer, and as predicted to be seen with recording electrodes from both types of simulations.

	L I	L II/III	L IV	L V	L VI
In microcircuit	0	.78	.89	.82	.91
Expected from Synaptic Input	0	.88	.96	.98	.92
Expected from Voltage Clamping	0	.84	.95	.97	.92

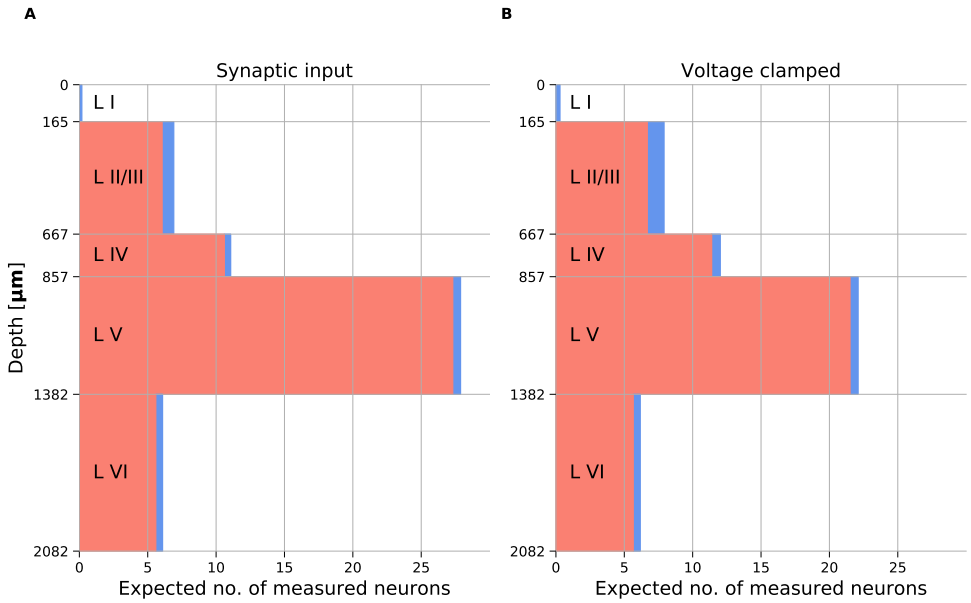

Figure 4.5: Expected number of measured neurons in each layer by synaptic input in **A**, and by voltage clamping in **B**. The expected numbers of excitatory and inhibitory neurons are in red and blue respectively. The vertical lengths of the bars are proportional to the thicknesses of the layers. The step functions are only approximately correct close to the edges, as the true curve will be a linear slope of less then 90 degrees at the border of a layer. This is due to there being fewer recordable neurons in the current layer at the borders, as well as signals from adjacent layers reaching into the current layer. These transition regions of the graph would be relatively small due to the thickness of the layers being much bigger than the recordable ranges of the spikes.

4.2 Morphology and maximum EAP amplitude

In this section, results from our investigation of effects of neuronal structure is presented. Specifically, the theory given in Pettersen and Einevoll (2008) [1], showing that maximum extracellular amplitude for a ball-and-stick neuron depends linearly on a morphology factor $\frac{d^{3/2}}{r_s}$, was tested on the Blue Brain models. Results from both synaptic input and voltage clamping are shown in Figure 4.6. A moderate to strong relationship was found with both methods, in particular when splitting the neurons into excitatory and inhibitory groups. When splitting, correlations of about 0.7 and 0.8 were found between amplitude and morphology factor. This suggests that the theory fits well also for active cells, as the correlation from synaptic input was marginally smaller than the correlation from voltage

clamping.

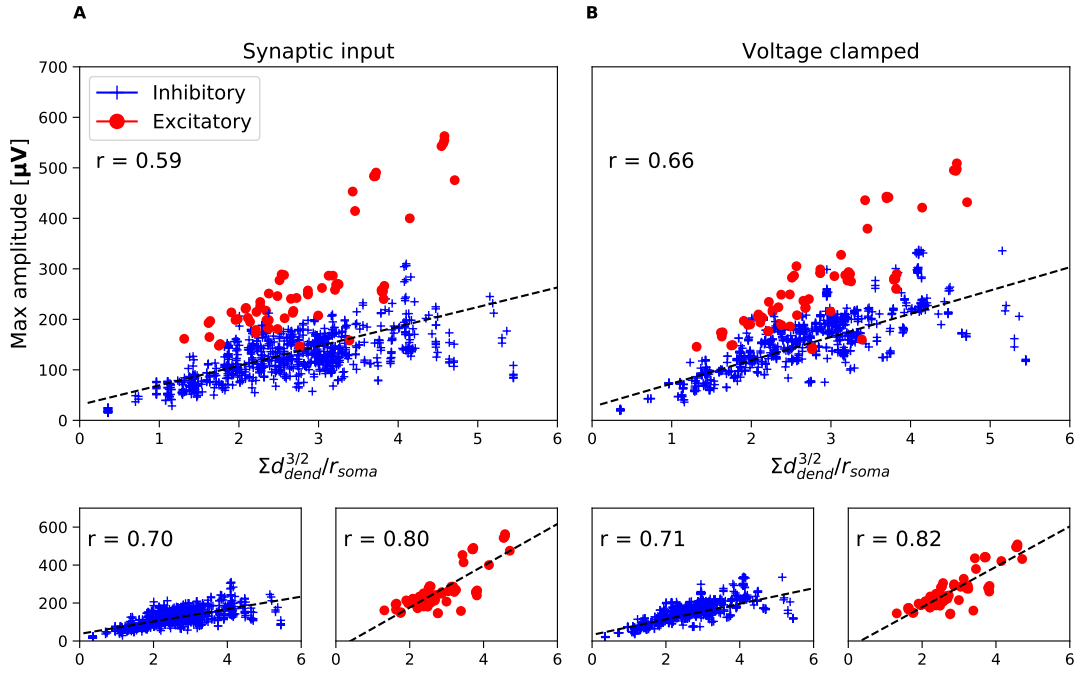

Figure 4.6: Maximum amplitude plotted against the morphology-factor $\frac{d^{3/2}}{r_s}$. Excitatory neurons are represented by red dots and inhibitory neurons by blue crosses. **A** and **B** show results from simulations using synaptic input and voltage clamping respectively. The upper plots show both groups of neuron together, and bottom plots separated. The dotted lines are linear regressions fitted to the plotted data, with r-values of the fits (correlations) in the upper left corners.

The results show a systematic difference between the maximum amplitudes of excitatory and inhibitory cell models of similar morphology factors. Simulations with idealised models were used in an attempt to uncover underlying reasons. In particular, a potential dependence on the number of dendrites attached to the soma was investigated. This was prompted by the difference in this figure between the sets of excitatory and inhibitory Blue Brain models. See Table 4.2 for an overview of some selected statistics of the cells in the microcircuit.

Ten idealised neuron models, with 1-10 equally long dendrites attached to soma were created, with the same morphology factor of 3.0. For simplicity, all cells had the same somatic radius of 4.0 μm, and all dendrites in a cell had the same diameter. A somatic spike was induced by voltage clamping, using a stored spike from a ball-and-stick model. Four electrodes were placed symmetrically at 1 μm

Table 4.2: Selected relevant means and standard errors of the Blue Brain excitatory (Exc.) and inhibitory (Inh.) cells.

	Soma radius [μm]	Dendrite diameter [μm]	No. of dendrites attached to soma	Morphology-factor
Exc. cells	5.29 ± 1.25	1.44 ± 0.816	8.09 ± 1.85	2.86 ± 0.825
Inh. cells	4.51 ± 1.05	1.52 ± 0.922	5.59 ± 1.99	2.55 ± 0.992

outside the soma, taking the average measured amplitude as the maximum EAP of the cell. The results are shown in Fig 4.7. They suggest that the maximum EAP of a cell depends on the number of dendrites on the soma, as the amplitude increased with more dendrites. In particular, from 1 to 2 dendrites the increase was more then two-fold. This is coherent with the results from the Blue Brain models, as excitatory neurons have larger EAP amplitudes and more dendrites on soma. An attempt to replicate the results from the simulation of the reconstructed models was carried out by using two sets of idealised cells with 8 and 5 dendrites, representing extracellular and inhibitory neurons respectively. Their somatic and dendritic radii were sampled from a normal distribution, with means and variances chosen such that the expected morphology factor was reasonably close to the average morphology factor in the Blue Brain set. When simulating the maximum EAP, a small gap was found between the groups with the "excitatory" cells generally having higher amplitudes relative to their morphology factor, see Figure 4.8.

The largest outliers in Figure 4.6 are excitatory neurons with morphology factors in the interval $[3, 5]$. These are mostly Layer V pyramidal cells, that generally have more dendrites on the soma than the average excitatory cell; for excitatory neurons in Layer V, the average was 9.35 ($\pm$1.25) dendrites, while the average across all layers was 8.09 ($\pm$1.85).

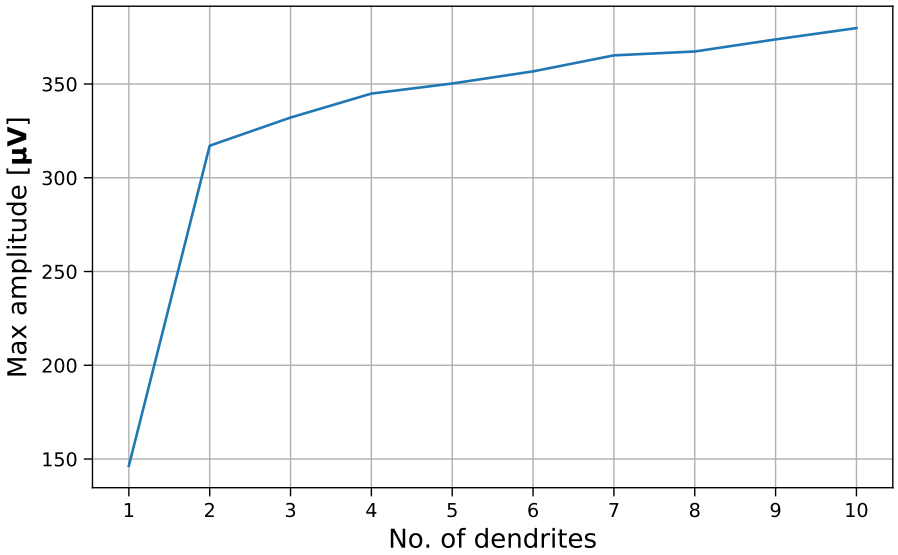

Figure 4.7: Maximum amplitudes of ten idealised cell models with equal morphology factors plotted against the number of dendrites on the soma. Morphology factor of 3.0 and soma radius of 4.0 μm were held constant for all models.

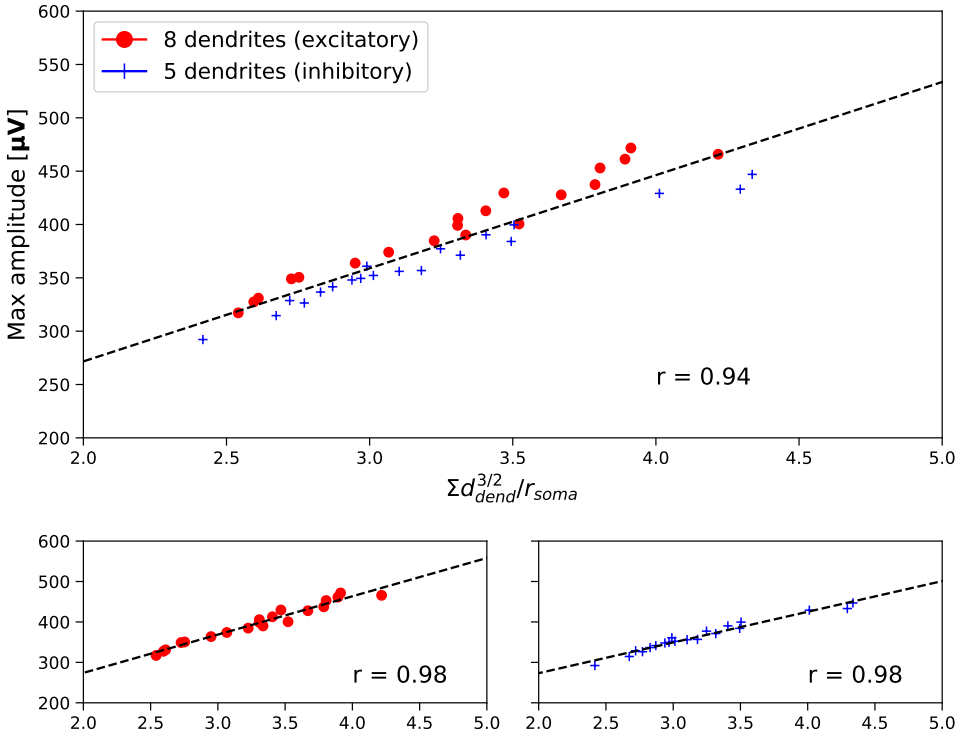

Figure 4.8: Maximum amplitude of two groups of neurons with 5 and 8 dendrites attached to soma plotted against morphology factor. The diameters of the dendrites and radii of the somas are sampled from a normal distribution. The top plot shows both groups of neurons together, and the bottom plots show them separated. The dotted lines are linear regressions fitted to the plotted points, with r-values (correlations) in the bottom right corners. The sets of cells with 8 and 5 dendrites are analogous to the Blue Brain excitatory and inhibitory models respectively.

Chapter 5

Discussion

Findings

EAPs from reconstructed neuron models were simulated in order to analyse a dependence on the basic cell structure, and make estimates of what one can expect to find with electrodes *in vivo*. We found nearly every neuron in the Blue Brain microcircuit to be detectable when recording immediately outside the soma, indicating that the proposed "dark matter problem" in the brain [10] is not caused by large numbers of neurons that are invisible to extracellular recordings.

By studying the spatial reach of signal for every cell in the microcircuit, estimates of how many neurons one can expect to record from in the somatosensory region of Wistar rat neocortex were made. The estimates are presented individually for each neocortical layer, and show that one would expect to record from about 20-30 neurons in Layer V, significantly more than in any other layer. The results suggest that the ratio of recorded excitatory to inhibitory neurons will be larger than the actual ratio present in tissue. Researchers we have spoken with have not noted such a wide discrepancy between the actual ratios and recorded ratios. [26, 27]. It is possible that excitatory neurons are less likely to be responding to the chosen stimuli, or that they simply have lower firing rates. These findings, and the insights into the detectable ranges of cells, can be useful to researchers working on recordings of extracellular potentials from living cells.

The proposed relationship between a morphology factor and maximum spike amplitude was studied by simulations of potentials immediately outside the soma surface of firing cell models. For the digitally reconstructed models, a strong rela-

tionship was found when analysing excitatory and inhibitory neurons individually. The results indicate that the findings in Pettersen and Einevoll (2008) [1] can be generalised to sets of more complex cells. The theory was derived for idealised models using voltage clamping, and here we did find that the theory fits slightly better to passive voltage clamped cells. But the results suggest that the theory generalises well to active cells receiving synaptic input. However, the picture remains incomplete, as for a given morphology factor excitatory neurons generally had higher EAP amplitudes than inhibitory neurons, in extreme cases by a factor of three (see Figure 4.6). The unexpected difference was studied by simulations on simple idealised models. The investigation hints at a connection to the number of dendrites attached to the soma, as it was shown that the maximum amplitudes increase with more dendrites for models of the same morphology factor. In the most extreme case, the amplitude increased by more than a factor of two, from one to two dendrites. A similar gap to the one between the reconstructed models were found using two idealised groups of cells with different numbers of dendrites. Even so, this is not a fully satisfactory explanation of the relatively large difference between the maximum amplitudes of the excitatory and inhibitory Blue Brain models.

Outlook

In future investigations, a process in which the reconstructed neurons are gradually simplified can be tried. Similarly, the idealised models can be gradually expanded upon to further resemble the reconstructed models. Then the simplest morphologies that accurately reproduce the results seen in Figure 4.6 can be analysed in order to determine the reasons behind the systematic difference in maximum amplitude.

A likely explanation is that there are systematic differences in the passive parameters between the excitatory and inhibitory neurons in the set of reconstructed models. These involve the axial resistances in the cell, the membrane capacitances and membrane resistances. As seen in Eq. 2.4, this will influence maximum extracellular spike amplitudes. We recently realized that the pyramidal cells were by design given a two-fold increase in their membrane capacitance to compensate for the effect of spines (not found on inhibitory cells) [28, 29]. Due to time constraints, we did not investigate this further. We suggest running similar simulations, with the passive parameters set equal for all cells, to determine the effect this may have on the amplitudes.

In summary, our results have shed new light on the connection between neuron morphologies and the corresponding amplitudes of the extracellular spikes, and suggested new directions for future research.

Bibliography

[1] K. H. Pettersen and G. T. Einevoll, 'Amplitude variability and extracellular low-pass filtering of neuronal spikes', *Biophysical Journal*, vol. 94, no. 3, pp. 784 –802, 2008.

[2] M. Bear, B. Connors and M. Paradiso, *NEUROSCIENCE: Exploring the Brain*, 4th ed. Wolters Kluwer, 2016.

[3] L. Chiu, Ed., *Brain Facts*, 8th ed. Society for Neuroscience, 2018.

[4] C. Koch, *What is consciousness?*, [Internet], https://www.nature.com/articles/d41586-018-05097-x, Last accessed: 2020-05-27. DOI: 10.1038/d41586-018-05097-x.

[5] G. Buzsáki, C. Anastassiou and C. Koch, 'The origin of extracellular fields and currents—eeg, ecog, lfp and spikes', *Nature reviews. Neuroscience*, vol. 13, pp. 407–20, May 2012.

[6] S. Lodato and P. Arlotta, 'Generating neuronal diversity in the mammalian cerebral cortex', *Annual Review of Cell and Developmental Biology*, vol. 31, no. 1, pp. 699–720, 2015.

[7] K. Pettersen, E. Hagen and G. Einevoll, 'Estimation of population firing rates and current source densities from laminar electrode recordings', *Journal of computational neuroscience*, vol. 24, pp. 291–313, 2008.

[8] D. H. Hubel and T. N. Wiesel, 'Receptive fields of single neurones in the cat's striate cortex', *The Journal of physiology*, vol. 148, no. 3, pp. 574–591, 1959.

[9] T. Hafting, M. Fyhn, S. Molden, M.-B. Moser and E. Moser, 'Microstructure of a spatial map in the entorhinal cortex', *Nature*, vol. 436, pp. 801–6, 2005.

[10] 'How silent is the brain: Is there a "dark matter" problem in neuroscience?', *Journal of Comparative Physiology A: Neuroethology, Sensory, Neural, and Behavioral Physiology*, vol. 192, no. 8, pp. 777–784, 2006.

[11] H. Markram *et al.*, 'Reconstruction and simulation of neocortical microcircuitry', *Cell*, vol. 163, no. 2, pp. 456 –492, 2015.

[12] S. Ramaswamy *et al.*, 'The neocortical microcircuit collaboration portal: A resource for rat somatosensory cortex', *Frontiers in Neural Circuits*, vol. 9, p. 44, 2015.

[13] S. Herculano-Houzel, 'The human brain in numbers: A linearly scaled-up primate brain', *Frontiers in Human Neuroscience*, vol. 3, p. 31, 2009.

[14] D. Sterratt, B. Graham, A. Gillies and D. Willshaw, *Principles of Computational Modelling in Neuroscience*. Cambridge University Press, 2011.

[15] A. L. Hodgkin and A. F. Huxley, 'A quantitative description of membrane current and its application to conduction and excitation in nerve', *Bulletin of Mathematical Biology*, vol. 52, no. 1, pp. 25–71, 1990.

[16] D. Amit and N. Brunel, 'Dynamics of a recurrent network of spiking neurons before and following learning', *Network: Comput Neural Syst*, vol. 8, 1998.

[17] P. Strata and R. Harvey, 'Dale's principle', *Brain Research Bulletin*, vol. 50, no. 5, pp. 349 –350, 1999.

[18] T. Carnevale and M. L. Hines, *The NEURON Book*. Cambridge University Press, 2006.

[19] R. Nunez P. L. Srinivasan, *Electric Fields of the Brain*. Oxford University Press, 2006.

[20] G. T. Einevoll, 'Extracellular potentials, forward modeling of', in *Encyclopedia of Computational Neuroscience*, D. Jaeger and R. Jung, Eds. Springer New York, 2015, pp. 1165–1168.

[21] H. Lindén, E. Hagen, S. Leski, E. Norheim, K. Pettersen and G. Einevoll, 'LFPy: A tool for biophysical simulation of extracellular potentials generated by detailed model neurons', *Frontiers in Neuroinformatics*, vol. 7, p. 41, 2014.

[22] G. R. Holt and C. Koch, 'Electrical interactions via the extracellular potential near cell bodies', *Journal of Computational Neuroscience*, vol. 6, no. 2, pp. 169–184, 1999.

[23] E. Hagen, S. Næss, T. V. Ness and G. T. Einevoll, 'Multimodal modeling of neural network activity: Computing lfp, ecog, eeg, and meg signals with lfpy 2.0', *Frontiers in Neuroinformatics*, vol. 12, p. 92, 2018.

[24] *Blue brain microcircuit portal*. [Online]. Available: http://bbp.epfl.ch/nmc-portal/.

[25] A. P. Buccino, T. V. Ness, G. T. Einevoll, G. Cauwenberghs and P. D. Häfliger, 'Localizing neuronal somata from multi-electrode array in-vivo recordings using deep learning', in *2017 39th Annual International Conference of the IEEE Engineering in Medicine and Biology Society (EMBC)*, 2017, pp. 974–977.

[26] K. Lensjø, Section for Physiology and Cell Biology, University of Oslo, Personal communication, 30th May 2020.

[27] A. P. Buccino, Department of Informatics, University of Oslo, Personal communication, 3rd Apr. 2020.

[28] E. Hay, S. Hill, F. Schürmann, H. Markram and I. Segev, 'Models of neocortical layer 5b pyramidal cells capturing a wide range of dendritic and perisomatic active properties', *PLOS Computational Biology*, pp. 1–18, 2011.

[29] C. Gold, D. A. Henze, C. Koch and G. Buzsáki, 'On the origin of the extracellular action potential waveform: A modeling study', *Journal of Neurophysiology*, vol. 95, no. 5, pp. 3113–3128, 2006.

Thank you.

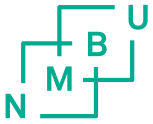

Norges miljø- og biovitenskapelige universitet
Noregs miljø- og biovitskapelege universitet
Norwegian University of Life Sciences

Postboks 5003
NO-1432 Ås
Norway